Near field optical tweezers

Smitha Kuriakose, Dru Morrish, Baohua Jia, James W.M. Chon, Xiasong Gan and Min Gu*
Centre for Micro-Photonics, Faculty of Engineering and Industrial Sciences, Swinburne University of Technology, PO Box 218, Hawthorn, VIC 3122

ABSTRACT

In this paper, we report on near field optical tweezers using focused evanescent illumination. The intensity pattern of the focused evanescent field has been characterized using a SNOM. The near field trapping efficiency has been experimentally and theoretically investigated using both TEM_{00} and TEM_{01} beams. The trapping efficiency was found to be polarization dependent and also changed for the two modes of illumination used. By incorporating the near field and far field optical tweezers one could construct an optical micromanipulation setup with great flexibility and accuracy, which would find applications in optical nanometry. By coupling the techniques like morphology dependent resonance (MDR), one could employ near field tweezers for near field sensing and for characterization of microfluidic channels.

Keywords: Trapping, near-field tweezers, focused evanescent illumination, morphology dependent resonance

1. INTRODUCTION

Since the pioneering work of Arthur Ashkin in 1970[1], optical tweezers have emerged as a powerful tool with enormous applications in physics and biology. The capabilities of optical traps have greatly evolved, incorporating different advanced techniques resulting in a wide range of applications[2-10]. In addition to being used as a tool to manipulate microscopic particles and molecules, theoretical and experimental work on the fundamental aspects of optical trapping are also being explored, providing new insights and information day by day.

Even though the far field optical tweezers could be remotely accessed and easily controlled, it is greatly desirable to reduce the trapping volume in far field while trying to study single molecule dynamics. One possible method would be to utilize the optical near field[11]. By using probes of dimensions significantly smaller than the illuminating wavelength, that is, the near field probes, one can monitor the non diffractive interaction of light with a sample in the immediate near field of probes used. The most popular near field probes used are the nano-aperture and the metallic tip. Around the year 2000, a few proposals were made to use the aperture type and the aperture less probes to construct near field laser tweezers[12-14]. Achieving near field tweezers using such geometries is practically challenging due to various reasons. The first and foremost challenge would be to position the sample accurately within the near field of the probe. It would be difficult to access the sample without damaging the probe. When a metallic tip is used as the near field probe, the heat generated could affect the stability of trapping. Even if we could construct such a near field trap, it would give only a low throughput.

An alternate method of generating a near field would be by using total internal reflection at the interface of two media. If light is incident from a denser to rarer medium, all the light incident at angles higher than the critical angle for the pair of media, would be total internally reflected and generate evanescent field. Recently we have demonstrated the construction of near field tweezers using a focused evanescent wave generated using a high numerical aperture objective[15]. Here the evanescent field is produced by a ring beam illumination. The size of the obstruction disk is chosen such that all the rays incident at angles less than the critical angle are cut off, resulting in a pure evanescent field. In this case, the gradient forces trap the particle laterally due to the ring nature of the beam and the axial forces push the particle towards the interface, resulting in a three dimensional trap. The advantage of this method is that a microparticle can be

*Phone: +61-3-9214 8776, email:mgu@swin.edu.au

Optical Trapping and Optical Micromanipulation II, edited by Kishan Dholakia, Gabriel C. Spalding
Proceedings of SPIE Vol. 5930 (SPIE, Bellingham, WA, 2005) · 0277-786X/05/$15 · doi: 10.1117/12.618617

thus confined to the center of the evanescent focal spot and therefore the manipulation of a trapped particle is possible with great flexibility and ease compared to that of using other near field probes. Due to the focused illumination, the evanescent wave strength is stronger than the evanescent field generated using total internal reflection on a prism. Also this does not generate any heating unlike in the case of using metallic probes. In addition to being used in near field tweezers, the focused evanescent wave has enormous applications in different fields like near field scanning imaging, non-linear microscopy, polarization microscopy, and superresolution.

2. THE FOCUSED EVANESCENT WAVE

In order to perform evanescent trapping, the NA 1.65 objective was chosen, as a reasonably wide ring beam was available to generate the near field. The objective used a special immersion oil of refractive index 1.78 and hence when water was used as the medium to suspend the microparticles, the critical angle for total internal reflection was 48 degrees and the maximum angle of convergence was 68 degrees, resulting in a sufficiently wide ring beam and high power to perform near field trapping (Figure 1).

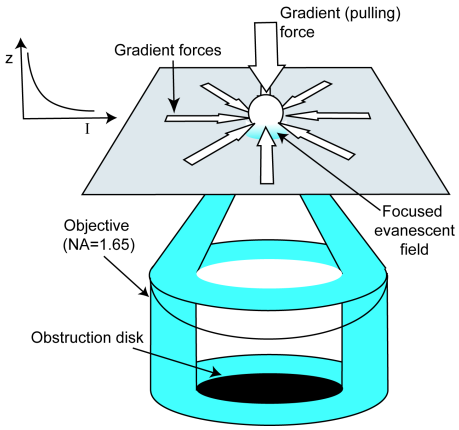

Figure1. Focused evanescent field generated for trapping the particle in near field

2.1. Characterization of the focused evanescent wave

A linearly polarized He–Ne laser beam was coupled into a high NA objective (Olympus, NA=1.65, 100X). A SNOM head (NTMDT) with an aluminium coated fiber probe vertical to the interface was placed on top of a cover glass. The tightly focused field was directly mapped with the fiber probe scanning in a transverse plane[16].

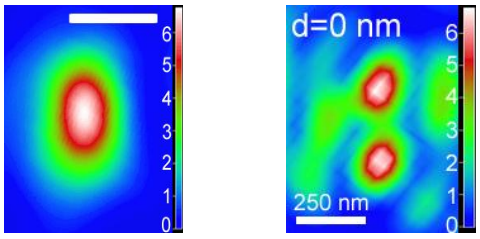

Figure 2. (a) The mapping of the intensity distribution in the focal region of an unobstructed beam, (b) the intensity distribution of a pure evanescent focus

Figure 2a shows the intensity distribution at the focus of an unobstructed beam. The focal spot is elongated as expected from the theoretical predictions[17-20] and experiments[21-24]. The direction of the incident polarization of the beam is as indicated by the arrow. Figure 2b shows the intensity distribution at the focus of a pure evanescent field generated by

using an obstruction disk of size 0.8, normalized with respect to the objective back aperture, where 0.6 is the critical obstruction size for total internal reflection at an air-glass interface. We can clearly see that the intensity distribution has two identifiable peaks along the direction of incident polarization. The peak intensity was measured at different distances from the interface and it was shown that the intensity showed an exponential decay with distance from the interface and the decay constant measured was in close agreement with the theoretical value of decay constant. This confirmed the evanescent nature of the field.

Another significant feature of the focused evanescent wave is the enhancement of the depolarization effect at the focus as a result of using a ring beam. There is a considerable enhancement of the longitudinal component of polarisation when we use the ring beam. Hence the incident and the longitudinal components dominate over the orthogonal component deciding the shape of the focal spot, resulting in a split-focus[25].

3. THEORETICAL MODELS FOR FOCUSED EVANESCENT TRAPPING

We have developed two theoretical models for focused evanescent trapping, one based on Ray Optics[26] and other based on Electromagnetic theory[27].

3.1. The Ray Optics (RO) Model

This Ray Optics model is an extension of Ashkin's Ray Optics Model to include the focused evanescent part of the illumination.

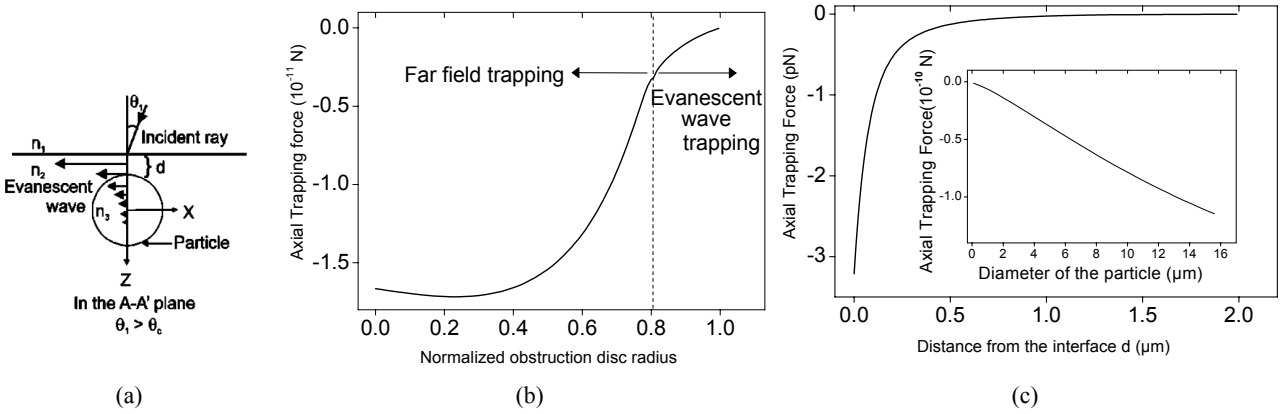

(a) (b) (c)

Figure 3. (a) A ray incident at the interface at a supercritical angle undergoes total internal reflection and gives rise to an evanescent wave that propagates on the interface and interacts with a particle with a strength decaying exponentially along the *Z* axis. (b) Lifting force as a function of the normalized obstruction radius ε for a particle of diameter 1 μm, immersed in water. λ = 532 nm. NA = 1.65. Incident power = 15 mW. (c) Lifting force as a function of the distance of the location of the particle from the interface ($\varepsilon = \varepsilon_{critical}$) The inset shows the lifting force as a function of the particle diameter.

We have considered an upright geometry of the setup used in figure 1 for the development of the RO model. A plane wave illumination focused by a high NA objective (NA=1.65) is incident on a particle of radius *a*, immersed in water. The refractive index of the cover slip of the 1.65 NA objective is 1.78. Therefore when the normalized obstruction radius ε, defined as the ratio of the radius of the disk to the radius of the back aperture of the objective, is greater than 0.806, light undergoes total internal reflection, generating evanescent field. The evanescent field was broken up into constituent rays as shown in Figure 3a, and the trapping force due to the interaction of each evanescent ray with the particle was calculated[26]. The net force due to a single ray was summed up to get the trapping force exerted by the whole beam. The dependence of the axial trapping force on the radius of the obstruction disk is demonstrated in Figure 3b. The negative value of the force means that the force points upward, confirming the lifting nature of the force in the upright trapping

system. The variation of the lifting force under focused evanescent illumination (ε > 0.8) with the distance of the location of the particle from the interface is demonstrated in Figure 3c. The lifting force is a maximum when the particle is at the interface and decreases with the increase in the distance of the particle from the interface, as may be expected for the decrease in the evanescent field. The inset in Figure 3c shows the variation of the lifting force with the particle size at $d = 0$. The magnitude of the force shows a linear increase with the particle size. As the particle size increases, the cross-sectional area of interaction of a small particle with the evanescent field also increases linearly, and this accounts for the linear relation between the particle size and the lifting force.

3.2. The Electromagnetic Model

We have used the vectorial diffraction theory to represent the highly focused field and its interaction with the particle. The electric and magnetic field components in the focal region of a high NA objective, in the second medium after the interface are given by[19],

$$\mathbf{E}_2(\mathbf{r}_p,-d) = -\frac{ik_1}{2\pi}\iint_{\Omega_1}\mathbf{c}(\phi_1,\phi_2,\theta)\exp\left\{ik_0\left[r_p\kappa+\Psi(\phi_1,\phi_2,-d)\right]\right\}\sin\phi_1 d\phi_1 d\theta \quad (1)$$

$$\mathbf{H}_2(\mathbf{r}_p,-d) = -\frac{ik_1}{2\pi}\iint_{\Omega_1}\mathbf{d}(\phi_1,\phi_2,\theta)\exp\left\{ik_0\left[r_p\kappa+\Psi(\phi_1,\phi_2,-d)\right]\right\}\sin\phi_1 d\phi_1 d\theta\,. \quad (2)$$

The indices 1 and 2 represent the two media and d represent the focal depth. ϕ_1 and ϕ_2 represent the angle of incidence and refraction at the interface, while k_0 and k_1 are the wave vectors in vaccum and in first medium respectively. $c(\phi_1,\phi_2,\theta)$, $d(\phi_1,\phi_2,\theta)$ and κ are defined in Ref [19]. $\psi(\phi_1,\phi_2,-d)$ is the spherical aberration function caused by the refractive index mismatch.

If we consider a homogenous microsphere located in medium 2 illuminated by the electromagnetic field given by equations 1 and 2, then the trapping force due to radiation pressure according to the steady state Maxwell stress tensor analysis is given by,

$$\langle\mathbf{F}\rangle = \frac{1}{4\pi}\int_0^{2\pi}\int_0^{\pi}\left\langle\left(\varepsilon_2 E_r\mathbf{E} + H_r\mathbf{H} - \frac{1}{2}\left(\varepsilon_2 E^2 + H^2\right)\hat{r}\right)\right\rangle r^2\sin\phi d\phi d\theta\,, \quad (3)$$

where, E_r and H_r are the radial components of the fields calculated on a spherical surface enclosing the particle, and r, θ and ϕ are the spherical polar co-ordinates.

The electromagnetic model was used to calculate the trapping efficiency for a small particle (a = 0.25 μm) and a big particle (a = 1 μm) along the direction of incident polarization. Figure 4 shows the trapping efficiency mapping, when a small and large polystyrene particle is transversally scanned in the X - direction across the focused evanescent field distribution, generated by placing a central obstruction (ε =0.85) perpendicularly to the path of an incoming laser beam, where ε =0.8 is the critical obstruction size to generate evanescent field. The trapping efficiency is related to the trapping force and power by $Q = Fc/n_2P$, where c is the speed of light in vacuum, n_2 is the surrounding medium refractive index, F is the trapping force and P is the incident power.

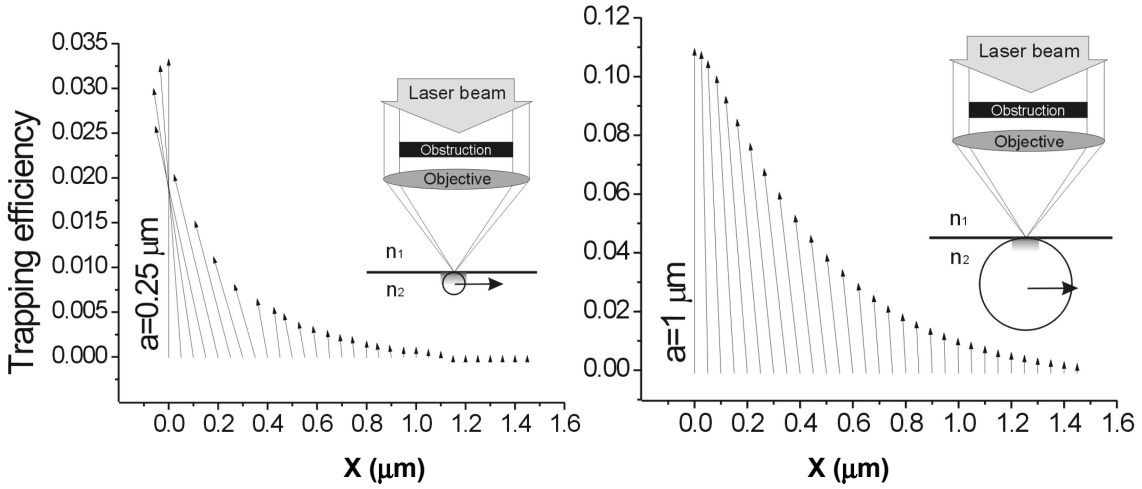

Fig. 4. Trapping efficiency mapping for a small and a large polystyrene particle of radius a, scanned in the X - direction (light polarization direction) across the focused evanescent field. NA = 1.65, λ = 532 nm, ε = 0.85, n_1 = 1.78 and n_2 = 1.33.

The calculations showed that the axial trapping efficiency was stronger for a big particle and also the decay rate of the axial trapping efficiency was less for a big particle, compared to the small particle. But, the transverse trapping efficiency was relatively stronger for a small particle than a big particle.

4. EXPERIMENTAL DETERMINATION OF THE TRANSVERSE TRAPPING EFFICIENCY

The transverse trapping efficiency was determined experimentally using a TEM_{00} beam. The experimental setup used is schematically shown in Figure 5. The collimated laser beam of wavelength 532 nm was directed onto the high NA objective, where it underwent total internal reflection and generating an evanescent field which was used to trap the 2μm beads. The trapping process was monitored by a CCD camera and the piezoelectric scanning stage for the sample holder was controlled electronically[28].

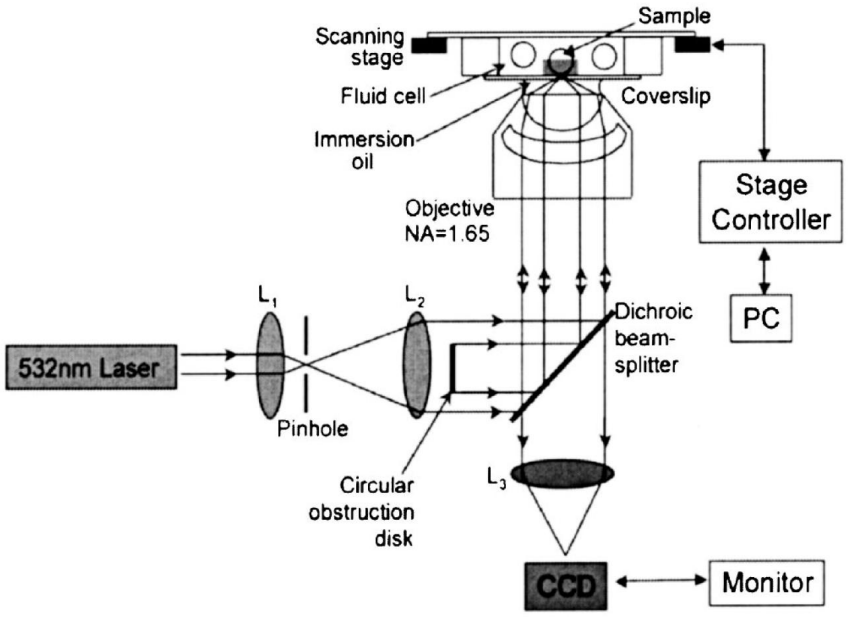

Figure. 5. A schematic diagram of an evanescent-field trapping system

The trapping force F is derived from the measured maximum translating velocity at which a trapping particle falls out of the trap and estimated by the Stokes law $F = 6\pi a\eta v$. Here a is the radius of a trapped particle, v is the maximum translation speed, and η is the viscosity of the surrounding medium. The dependence of transverse trapping efficiency on the size of obstruction disk was analyzed (Figure 6) by scanning the particle along directions parallel and perpendicular to the incident polarization. The maximal TTE decreases with the size of obstruction disk due to the decreasing contribution from propagating components. The TTE decreases at a rate very close to what predicted by the theory for both the directions. Also the maximal TTE for an unobstructed beam for the direction parallel to the incident polarization is higher than the other by about 12%. As we approach the near field, the TTE is almost the same for both scanning directions.

For the 2μm bead there was good match between the theory and the experiment but when we calculated the TTE for smaller particles, there was a deviation from the prediction of theory in the near field regime. This could be attributed to factors such as multiple reflections from the interface, Brownian motion and the strong axial force which are not accounted for in the theory.

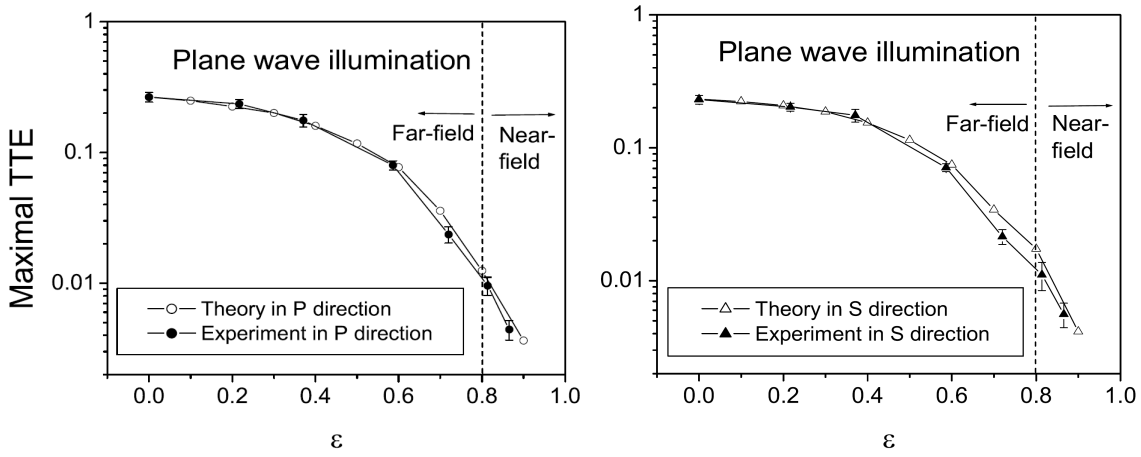

Fig. 6. The calculated and measured maximal TTE of a polystyrene particle of 1 μm in radius as a function of the obstruction size ε for *P* and *S* scanning directions under plane wave illumination.

Experiments were done for calculating the TTE for a TEM_{01} beam[28], which showed good agreement with the calculations, but the TTE for an unobstructed beam was 1.4 times less than that for plane wave illumination.

5. CONCLUSION

In summary, near field optical tweezers is a promising tool for optical nanometry. We have performed the characterization of the focused evanescent wave and determined the near field trapping efficiency for microscopic dielectric particles using TEM_{00} and TEM_{01} beams. We have also developed two theoretical models, a Ray Optics (RO) Model and an Electromagnetic (EM) Model to study the near field tweezers using a focused evanescent wave. The far field tweezers have already been able to monitor movements of molecules like myosin, kinesin and DNA with very high resolution. By using near field tweezers it would be possible to further improve the optical micromanipulation resolution to nanometer scale. By incorporating the far field and near field trapping geometries together, one would be able to create a micromanipulation setup with great flexibility and accuracy. Also by incorporating techniques like morphology dependent resonance (MDR), near field tweezers could be advantageous for near field sensing and characterization of microfluidic channels.

REFERENCES

1. A. Ashkin, Phys.Rev.Lett. **24**, 156 (1970).
2. A. D. Mehta *et al.*, Science **283**, 1689 (1999).
3. A. Ishijima and T. Yanagida, Trends Biochem. Sci. **26**, 438 (2001).
4. Y. Ishii, A. Ishijima, and T. Yanagida, Trends Biotechnol. **19**, 211 (2001).
5. D. G. Grier, Nature (London) **424**, 810 (2003).
6. P. T. Korda, M. B. Taylor, and D. G. Grier, Phys. Rev. Lett. **89**, 128301 (2002).
7. B. Onoa *et al.*, Science **299**, 1892 (2003).
8. T. T. Perkins *et al.*, Science **264**, 822 (1994).
9. T. T. Perkins, D. E. Smith, and S. Chu, Science **264**, 819 (1994).
10. J. C. Crocker and D. G. Grier, Phys. Rev. Lett. **77**, 1897 (1996).
11. M.Ohtsu and K.Kobayashi, *Optical Near fields*, (Springer, Heidelberg, 2004).
12. L. Novotny, R.X.Bian, and X.S.Xie, Phys. Rev. Lett. **79**, 645-648 (1997).
13. K. Okamoto and S. Kawata, Phys. Rev. Lett. **83**, 4534-4537 (1999).
14. Chaumet, Rahmani, Nieto-Vesperinas, Phys. Rev. Lett. **88,** 123601 (2002).
15. Min Gu, Jean-Baptiste Haumonte, James Chon, Xiaosong Gan, Appl. Phys. Lett., **84**, 4236-4238 (2004).
16. Baohua Jia, Xiaosong Gan, and Min Gu, Appl. Phys. Lett. **86**, 131110 (2005).
17. B. Richards and E. Wolf, Proc. R. Soc. London, Ser. A **253**, 358 (1959).
18. C. J. R. Sheppard, Optik (Stuttgart) **48**, 329 (1977).
19. P. Torok, P. Varga, Z. Laczik, and G. R. Booker, J. Opt. Soc. Am. A **12**, 325 (1995).
20. M. Gu, *Advanced Optical Imaging Theory* (Springer, Heidelberg, 2000).
21. J. W. M. Chon, M. Gu, C. Bullen, and P. Mulvaney, Opt. Lett. **28**, 1930 (2003).
22. K. Bahlmann and S. W. Hell, J. Microsc. **200**, 59 (2000).
23. K. Bahlmann and S. W. Hell, Appl. Phys. Lett. **77**, 612 (2000).
24. R. Dorn, S. Quabis, and G. Leuchs, J. Mod. Opt. **50**, 1917 (2003).
25. J.W. M. Chon, Xiaosong Gan and Min Gu, App. Phys. Lett. **81**, 9 (2002)
26. Smitha Kuriakose, Xiasong Gan, James W. M. Chon, and Min Gu, J. Appl. Phys. **97**, 083103 (2005)
27. Djenan Ganic, Xiaosong Gan, and Min Gu, Opt. Exp. **12,** 2670-2675 (2004)
28. Djenan Ganic, Xiaosong Gan, and Min Gu, Opt. Exp. **12**, 5533-5538 (2004),